This is an open access article published under an ACS AuthorChoice License, which permits copying and redistribution of the article or any adaptations for non-commercial purposes.

ACS OMEGA

Article

Cite This: ACS Omega 2019, 4, 13400−13407

http://pubs.acs.org/journal/acsodf

β-$SnWO_4$ with Morphology-Controlled Synthesis and Facet-Depending Photocatalysis

Lucas Warmuth and Claus Feldmann*

Institute of Inorganic Chemistry, Karlsruhe Institute of Technology (KIT), Engesserstraße 15, 76131 Karlsruhe, Germany

Supporting Information

ABSTRACT: Faceted β-$SnWO_4$ microcrystals are prepared with different morphologies including tetrahedra, truncated tetrahedra, truncated octahedra, and short-spiked and long-spiked spikecubes. All of these morphologies are prepared with comparable experimental conditions via microwave-assisted synthesis of high-boiling alcohols (the so-called polyol method). The decisive parameters for controlled formation of one or the other morphology of faceted β-$SnWO_4$ microcrystals are studied and discussed, including microwave-assisted heating, $Sn(OH)_2$ as the Sn^{2+} reservoir, the temperature of particle nucleation, the temperature of particle growth, and the concentration of the starting materials. Morphology and crystallinity are characterized by scanning electron microscopy, X-ray powder diffraction, UV−vis, and Fourier-transform infrared spectroscopy. Finally, the photocatalytic properties of all obtained faceted microcrystals—tetrahedra, truncated tetrahedra, truncated octahedra, cubes, and short-spiked and long-spiked spikecubes—are exemplarily compared with regard to the photocatalytic decomposition of rhodamine B and the influence of the respective surface crystal planes.

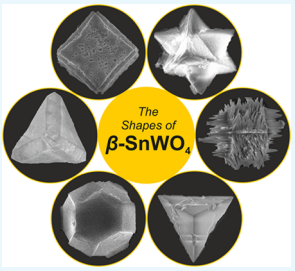

Downloaded via KIT BIBLIOTHEK on September 10, 2019 at 09:52:19 (UTC).
See https://pubs.acs.org/sharingguidelines for options on how to legitimately share published articles.

INTRODUCTION

Prerequisites for efficient photocatalysts essentially comprise a high specific surface area as well as high crystallinity.[1,2] A high specific surface area ensures fast diffusion to and fast conversion of the reactants at the photocatalyst surface. High crystallinity guarantees efficient generation of electron−hole pairs after light absorption at the lowest level of defect-related loss processes. Optimizing these features causes conflicting issues and either results in high-surface nanoparticles or low-defect single crystals. Faceted microcrystals turned out as the most promising compromise, exposing highly reactive crystal facets.[1,2] The reactivity of specific facets, however, can differ dramatically, e.g., due to different redox activity or different adsorption/desorption processes of reactants/products.

The realization of faceted microcrystals needs efficient control of nucleation and growth processes, including precise adjustment of the decisive reaction parameters (e.g., concentrations, temperature) and use of selected surface-active agents to block or to support the growth of specific crystal facets.[1,2] So far, tailored growth and formation mechanism of faceted nano- and microcrystals were most widely studied for zerovalent metals.[3,4] In comparison to metals, much less is known regarding the growth of faceted metal-oxide microcrystals. Most often, non-Platonian shapes such as rods, plates, flakes, lenses, flowers, etc. were described. With regard to Platonian shapes such as tetrahedra, octahedra, or cubes, typically, only a single faceted morphology can be obtained at specific conditions of synthesis (e.g., ZnO, Cu_2O, Ag_2O, TiO_2, CeO_2, Fe_2O_3).[5−9] Obtaining faceted microcrystals with different Platonian shapes at comparable conditions of reaction is even more limited and predominately related to Cu_2O, TiO_2, MoO_x, CeO_2, and $SrTiO_3$.[10−15] In particular, tetrahedral shapes, to our surprise, were yet rarely described, for instance, in the case of CdSe or Ag_3PO_4.[16,17]

With regard to visible-light-driven metal-oxide photocatalysts, β-$SnWO_4$[18,19] recently turned out as an interesting material and promising addition to $BiVO_4$,[20,21] as an intensely studied visible-light-driven photocatalyst, and anatase-TiO_2,[22] as the most widely studied but UV-excited photocatalyst. Yellow β-$SnWO_4$ with a direct band gap of 2.7 eV, in fact, is a high-temperature modification (>670 °C)[18,23] that we could reliably prepare as a metastable compound near room temperature only recently.[18,24] So far, synthesis of high-boiling, multivalent alcohols (so-called polyol synthesis)[25] only resulted in high-surface but low-crystallinity nanoparticles that nevertheless turned out promising for photodynamic treatment of tumor cells.[26] Moreover, faceted dodecahedral β-$SnWO_4$ microcrystals were realized in low quantities by microemulsion synthesis.[18] Finally, we could recently realize β-$SnWO_4$ with a unique spikecube-type morphology.[27]

Motivated by the peculiar shape of the β-$SnWO_4$ spikecubes, we intended to examine the conditions of nucleation and growth more detailedly. Moreover, we aimed at understanding the conditions of growth and eventually realizing further faceted shapes of β-$SnWO_4$. As a result, widespread faceted morphologies are selectively grown for the first time, including tetrahedra, truncated tetrahedra, truncated octahedra, cubes, and spikecubes. These faceted microcrystals are obtained by microwave-assisted polyol synthesis. Finally, the photocatalytic

Received: May 31, 2019
Accepted: July 4, 2019
Published: August 1, 2019

© 2019 American Chemical Society

DOI: 10.1021/acsomega.9b01593
ACS Omega 2019, 4, 13400−13407

Table 1. Temperature Conditions and Concentration of Starting Materials for the Growth of Faceted β-$SnWO_4$ Microcrystals

morphology	nucleation temperature, T_N (°C)	growth temperature, T_G (°C)	concentration of starting materials (mmol/L)	speed of heating ($T_N \rightarrow T_G$) (min)
tetrahedra	80	180	5	1
truncated tetrahedra	80	180	17	20
truncated octahedra	200	200	17	1
spikecubes (short-spiked)	80	170	24	1
spikecubes (long-spiked)	80	180	24	1

activity is conceptually studied by decomposition of rhodamine B, and it clearly evidences a facet-depending performance.

RESULTS AND DISCUSSION

Synthesis and Crystallinity. Crystallinity is a prerequisite for morphology control and the formation of faceted microcrystals, in general. Aiming at the yellow, cubic β-$SnWO_4$, two fundamental limitations for controlled crystal growth are relevant. On the one hand, β-$SnWO_4$ remains amorphous if the temperature of particle nucleation and particle growth is too low. High temperatures, on the other hand, favor the formation of the thermodynamically more stable red, orthorhombic α-$SnWO_4$ phase. Based on Jeitschko's first report on the crystal structure,[23] we already made many efforts on obtaining faceted microcrystals of the metastable β-$SnWO_4$. Low-temperature synthesis indeed resulted in well-defined but low crystalline, spherical nanoparticles in a size range of 5−20 nm.[18,26] Synthesis of multivalent, high-boiling alcohols recently allowed realizing the so-called β-$SnWO_4$ spikecubes, i.e., cubes on whose surfaces spikes were grown in addition.[27] The availability of this unique morphology also promises the option to obtain further interesting morphologies.

Based on our previous experiments, first of all, we have concentrated on how to crystallize β-$SnWO_4$ based on the fact that crystallinity is a prerequisite for obtaining specific morphologies and faceted microcrystals. For all experiments, $SnCl_2{\cdot}2H_2O$ and $Na_2WO_4{\cdot}2H_2O$ were used as the starting materials. Na_2WO_4 is essential due to the presence of tetrahedrally coordinated $[WO_4]^{2-}$, which is also the building unit in β-$SnWO_4$.[18] In contrast, only α-$SnWO_4$ was obtained as the crystalline phase at any temperature if octahedrally coordinated (WO_6) units were available in the starting material (e.g., $(NH_4)_6Mo_7O_{24}$).[18] Moreover, diethylene glycol (DEG) was used as the solvent. Finally, the amount of water as a mineralizer was kept constant at 6 mL of water per 150 mL of DEG (see the Experimental Section). Based on these fixed conditions, the concentration of the starting materials and especially the temperature treatment were modified (Table 1).

With regard to the temperature, it needs to be noticed that only β-$SnWO_4$ nanoparticles of low crystallinity were obtained if the temperature was <170 °C. Below this threshold, scanning electron microscopy (SEM) clearly indicates the presence of spherical nanoparticles with a diameter <100 nm (Figure 1). X-ray powder diffraction (XRD), moreover, indicates the low crystallinity with only the most intense Bragg peak being observable with a low intensity and a broad peak width (Figure 1). Thus, a temperature ≥170 °C is indispensible for crystallization. Temperatures >220 °C, however, result in decomposition of DEG, which proceeds faster with higher temperature and longer time of heating.[25] As a result, the temperature window for successful crystallization and controlled growth of faceted β-$SnWO_4$ microcrystals is limited to ≥170 and ≤220 °C.

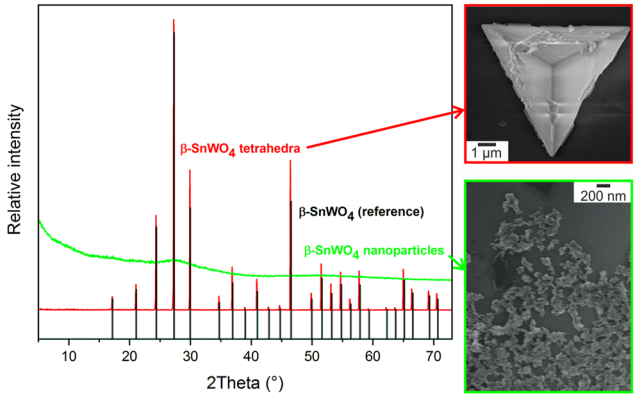

Figure 1. Crystallinity and phase composition of β-$SnWO_4$ according to XRD and SEM: amorphous β-$SnWO_4$ nanoparticles (obtained at a nucleation temperature T_N < 170 °C) and faceted β-$SnWO_4$ microcrystals (obtained at a nucleation temperature T_N ≥ 170 °C; β-$SnWO_4$ tetrahedra shown as representative example of microcrystals). Bulk-β-$SnWO_4$ shown as a reference (ICSD no. 00-070-1497).

Indeed all faceted β-$SnWO_4$ microcrystals, including tetrahedra, truncated tetrahedra, truncated octahedra, and short-spiked and long-spiked spikecubes were obtained in the 170−220 °C temperature window. Prior to the detailed elucidation of the growth conditions, the faceted β-$SnWO_4$ microcrystals were also characterized by optical spectroscopy (UV−vis) and Fourier-transform infrared (FT-IR) spectroscopy (Figure 2). Since the respective spectra were similar for all faceted microcrystals, β-$SnWO_4$ tetrahedra are exemplarily illustrated here. According to UV−vis spectra, β-$SnWO_4$ microcrystals show the expected absorption in the near ultraviolet to blue spectral regime (<500 nm, Figure 2a). Based on Tauc plots, band gaps of 2.7−2.9 eV were determined (Supporting Information (SI): Figure S1), which is in good agreement with the previously reported data of β-$SnWO_4$ spikecubes (2.9 eV).[27] Photoluminescence spectra, furthermore, exclude fluorescence as a relevant competitive loss process for photocatalysis (SI: Figure S2). FT-IR spectra of β-$SnWO_4$ indicate vibrations at 1050−700 cm^{-1} (Figure 2b), which can be assigned to the orthotungstate anion $[WO_4]^{2-}$ and which compare well with Na_2WO_4 as a reference.[28] Additional vibrations relate to adsorbed water (ν(O−H): 3400−3300 cm^{-1}, $\delta(H_2O)$: 1650 cm^{-1}). Even more important, FT-IR spectra of the β-$SnWO_4$ microcrystals did not show any vibrations related to adhered DEG after purification (Figure 2b), which is highly relevant for photocatalysis since adhered, surface-active molecules could block the active surface and thus reduce the catalytic activity. The

DOI: 10.1021/acsomega.9b01593
ACS Omega 2019, 4, 13400−13407

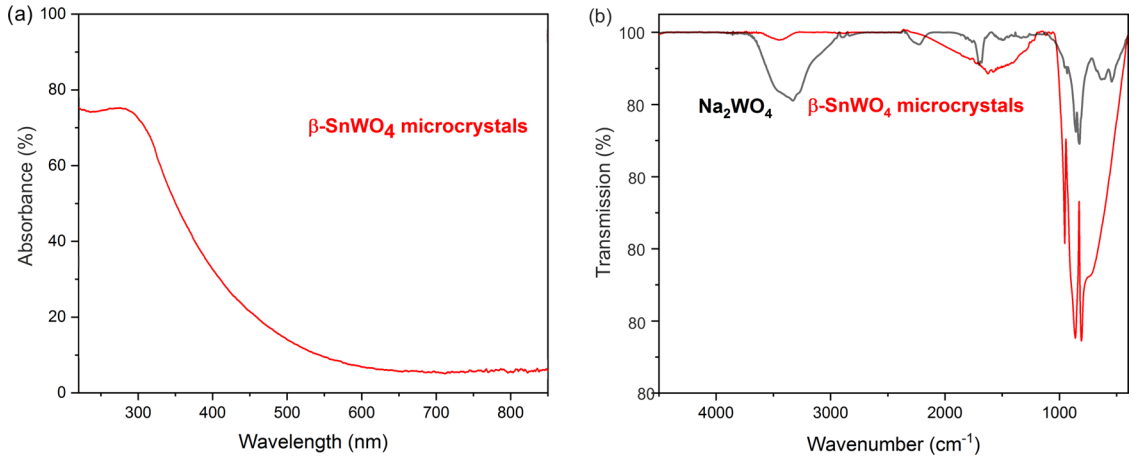

Figure 2. Spectroscopic characterization of β-$SnWO_4$ microcrystals (β-$SnWO_4$ tetrahedra shown as a representative example of microcrystals; for other morphologies see Figure S1 in the SI): (a) UV−vis spectrum; (b) FT-IR spectra (Na_2WO_4 as a reference).

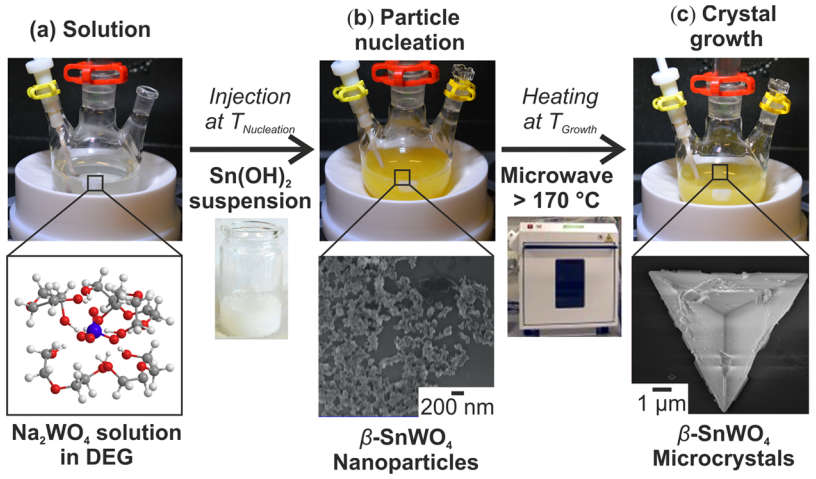

Figure 3. Schematic illustration of the microwave-assisted growth of faceted β-$SnWO_4$ microcrystals: (a) solution of Na_2WO_4 in DEG; (b) nucleation of β-$SnWO_4$ nanoparticles subsequent to the injection of an aqueous $Sn(OH)_2$ suspension at the nucleation temperature T_N (Table 1); (c) microwave-assisted growth of faceted β-$SnWO_4$ microcrystals at the growth temperature T_G (Table 1).

fact that the optical properties, band gap, and surface functionalization are identical for all faceted β-$SnWO_4$ microcrystals within the experimental significance is highly important for the latter comparison of the photocatalytic properties.

Morphology Control. The strategy to obtain faceted β-$SnWO_4$ microcrystals comprises two sequential steps. First of all, the nucleation of β-$SnWO_4$ was initiated at the nucleation temperature T_N (Table 1, Figure 3b). Thereafter, crystallization and controlled growth proceed at the growth temperature T_G (Table 1, Figure 3c). T_N was adjusted with regard to two aspects. On the one hand, nucleation as an endothermal process can be supported by elevated temperatures, resulting in a T_N value higher than room temperature. Since $Na_2WO_4{\cdot}2H_2O$ is only completely dissolved in DEG at temperatures >70 °C (Figure 3a), T_N was typically set to 80 °C. At this temperature, moreover, the injection of aqueous $SnCl_2{\cdot}2H_2O$ did not cause any retardation of boiling. Here, it needs to be noticed that dissolving $SnCl_2{\cdot}2H_2O$ in water at neutral pH results in a suspension of $Sn(OH)_2$ (Figure 3a; SI: Figure S3). However, the addition of a $Sn(OH)_2$ suspension turned out to be essential for subsequent controlled growth. After injection of the aqueous $Sn(OH)_2$ suspension into the solution of $Na_2WO_4{\cdot}2H_2O$ in DEG, not all Sn^{2+} is instantaneously available for the nucleation of β-$SnWO_4$, since $Sn(OH)_2$ dissolves only slowly and remains in the suspension as the Sn^{2+} reservoir. In terms of the LaMer−Dinegar model,[29] thus, the supersaturation is kept low and results in a low nucleation rate of β-$SnWO_4$.

Subsequent to the nucleation of β-$SnWO_4$, crystallization and faceted growth were performed at 170 °C $\geq T_G \leq$ 220 °C (Table 1, Figure 3c). Since $Sn(OH)_2$ is still available as an Sn^{2+} reservoir, its proceeding dissolution leads to continuous growth of the β-$SnWO_4$ nuclei. According to the LaMer−Dinegar model,[29] the exothermal growth reaction should preferentially be performed at lower temperature than the nucleation (i.e., <80 °C). High temperatures (≥170 °C), however, are essentially needed for crystallization. These conflicting issues were addressed by fast, microwave-assisted heating from T_N to T_G (Figure 3c). Both measures together—slow dissolution of $Sn(OH)_2$ and fast microwave-assisted heating—guarantee for tailored growth. The slow dissolution of $Sn(OH)_2$ also provides a sufficient amount of water as a mineralizer even at high temperature (≥170 °C). Finally, it needs to be noticed that the temperature for crystallization and the duration of heating are closely correlated. Thus, 2 h of

DOI: 10.1021/acsomega.9b01593
ACS Omega 2019, 4, 13400−13407

heating are required at 170 °C whereas only 15 min are sufficient at 200 °C (Table 1). DEG as a coordinating solvent gurantees sufficient surface stabilization of the growing β-$SnWO_4$ microcrystals. The proceeding growth of the microcrystals can be followed even by the naked eye. After finishing the nucleation, the yellow color of the β-$SnWO_4$ suspension brightens up, which originates from the high reflectivity of the microcrystal surface facets (Figure 3b,c).

Based on the general consideration of the synthesis strategy, the first parameter to be modified for controlled growth relates to the injection of the $Sn(OH_2)$ suspension and T_N. Accordingly, tetrahedra and truncated tetrahedra were obtained at T_N = 80 °C (Table 1, Figure 4a), whereas

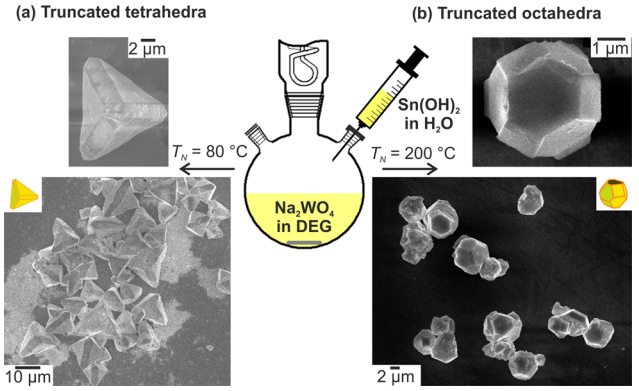

Figure 4. Growth of truncated tetrahedra (a) and truncated β-$SnWO_4$ octahedra (b) depending on the nucleation temperature T_N of the starting material added according to SEM images (overview and detailed images for each sample).

truncated octahedra were formed at a T_N of 200−220 °C (Table 1, Figure 4b). In terms of the crystal facets, the {111} crystal plane is obviously preferred over the {100} crystal plane at low temperatures. According to Ostwald's step rule, therefore, the {111} crystal plane has to be considered as more reactive than the {100} crystal plane.

As a second parameter, the concentration of the starting materials turned out to be useful for facet engineering (Figure 5). At low concentration (5 mmol/L), β-$SnWO_4$ tetrahedra only exposing {111} crystal planes were obtained (Figure 5a,d). In few cases, moreover, twinned tetrahedral growth was observed, resulting in so-called star tetrahedra (Figure 5f). Upon increasing the concentration (17 mmol/L), {100} crystal planes occur in addition to {111} crystal planes, which results in truncated tetrahedra (Figure 5b,e). Finally, a further increase of the concentration of the starting materials (24 mmol/L) leads to β-$SnWO_4$ cubes and spikecubes (Figure 5c). Here, the initial cubes expose {100} crystal facets only. At this concentration, the dissolution of $Sn(OH)_2$ obviously provides more Sn^{2+} than is removed from the solution by crystal growth. As a result, additional $SnWO_4$ nuclei are formed that adhere on the surface of the already existing cubes. The hindered growth of these surface-adhered nuclei thereafter allows only one edge of a new cube to grow, which results in spikes.

The length of the spikes can be controlled by the time left for growth at T_G as the third relevant parameter (Figure 6). If the time at 170 °C was limited to 2 h, followed by rapid cooling to room temperature, almost no spikes occur on the surface of the β-$SnWO_4$ cubes (Figure 6a). Rapid cooling was

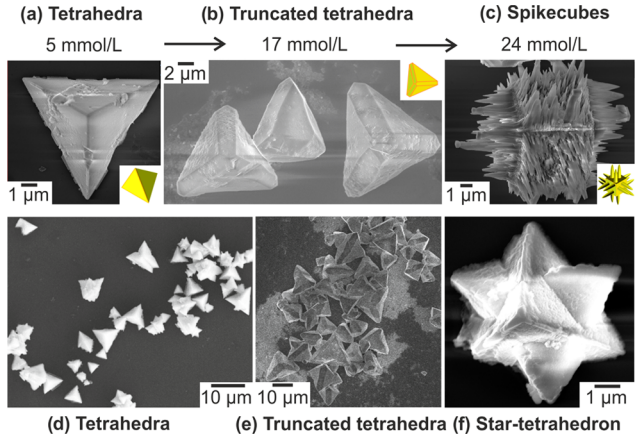

Figure 5. Growth of tetrahedra (a, d), truncated tetrahedra (b, e), and β-$SnWO_4$ spikecubes (c) depending on the concentration of the starting materials according to SEM images ((d, e) overview images; (f) star tetrahedra occur with about 1−3% in samples of β-$SnWO_4$ tetrahedra).

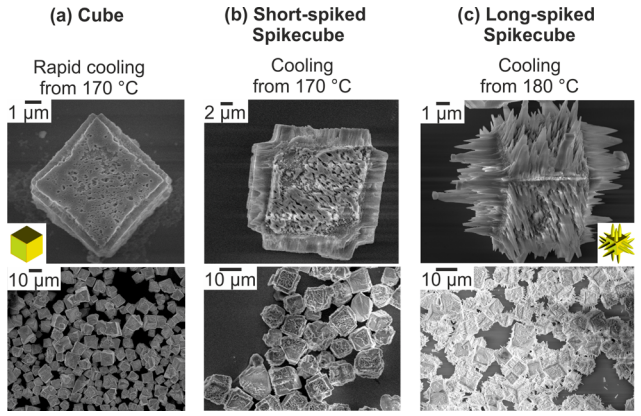

Figure 6. Growth of β-$SnWO_4$ cubes (a), short-spiked (b) and long-spiked (c) β-$SnWO_4$ spikecubes depending on the cooling procedure according to SEM images (overview and detailed images for each sample).

performed by extracting certain volume (5 mL) of the suspension and subsequent injection into water (10 mL) at room temperature. In the case of slow natural cooling to room temperature (about 60 min), the spikes become longer and result in short-spiked spikecubes (Figure 6b). If the growth of the spikes started at a higher temperature (180 °C), followed by slow natural cooling, finally, long-spiked spikecubes were realized (Figure 6c).

Taken together, the growth of β-$SnWO_4$ starts with {111} crystal planes resulting in tetrahedra. If the growth proceeds for a longer period, the {100} crystal planes become dominating, which results in truncated tetrahedra and thereafter in cubes. If growth and nucleation are parallel, then nuclei adhere on the existing cubes and grow into spikecubes. If, in contrast, the nucleation was already performed at high temperature (220 °C)—thus at high activation energy—{111} and {100} directly occur in parallel, resulting in the growth of truncated octahedra. Hence, the faceted microcrystals follow a well-controlled growth pattern.

Photocatalytic Evaluation. To evaluate the properties of the faceted β-$SnWO_4$ microcrystals, photocatalysis is an obvious tool. To allow a direct comparison of the differently

DOI: 10.1021/acsomega.9b01593
ACS Omega 2019, 4, 13400−13407

shaped microcrystals, the experiments were performed at identical conditions. Thus, identical concentrations of the respective β-$SnWO_4$ microcrystals (0.18 g/L) were suspended in water, and identical concentrations of zwitterionic rhodamine B (RhB, 0.20 mg/L) were added. RhB was selected, on the one hand, since its absorption (500−600 nm, SI: Figure S4) is different from the absorption of β-$SnWO_4$ (<500 nm, Figure 2). On the other hand, the adhesion of the zwitterionic RhB on the photocatalyst surface is independent from eventual charging of the respective surface of the photocatalyst. After adjusting the respective suspensions, the absorption of RhB at λ_{RhB} = 554 nm was continuously monitored under artificial daylight (AM 1.5G solar light, 100 mW/cm^2) (Figure 7). First

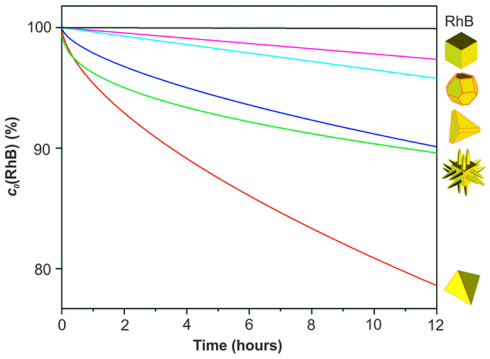

Figure 7. Photocatalytic RhB degradation depending on the morphology of the faceted β-$SnWO_4$ microcrystals (RhB: autophotolysis of rhodamine B; $c_{0,RhB}$: initial rhodamine B concentration of 0.18 g/L; β-$SnWO_4$ in all cases with a concentration of 0.20 mg/L).

of all, the autophotolysis of RhB (in the absence of any photocatalyst) was verified and showed no considerable effect within the significance of the experiment. With regard to the faceted β-$SnWO_4$ microcrystals, cubes and truncated octahedra show the lowest activity followed by truncated tetrahedra and long-spiked spikecubes (Figure 7). By far, the highest photocatalytical activity is observed for the tetrahedra.

To explain the different photocatalytic performance of the faceted β-$SnWO_4$ microcrystals, first of all, it needs to be considered that several conditions were more-or-less identical, including the concentration of β-$SnWO_4$ and RhB as well as the crystallinity, optical absorption, and band gap of the microcrystals (Figure 2; SI: Figures S1 and S2). Moreover, the size of the microcrystals were very comparable ranging from the truncated octahedra (4−6 μm) as the smallest to the truncated tetrahedra (10−16 μm) as the largest species (Table 2). Furthermore, nitrogen sorption measurements were performed to determine the specific surface according to the Brunauer−Emmett−Teller formalism. As a result, values between 1 and 3 m^2/g were obtained that are again very similar. Finally, the ζ-potential was measured to evaluate the influence of surface charging. Hence, all β-$SnWO_4$ microcrystals show negative charging with values from −24 to −43 mV at pH = 7 (Table 2). Despite certain differences of the faceted microcrystals, size, specific surface area, and surface charging cannot explain the observed photocatalytic activity coherently (Table 2).

With regard to a great number of very comparable features of the faceted β-$SnWO_4$ microcrystals that cannot explain the photocatalyic performance, there is only one decisive aspect left—the nature of the crystal-surface facets. In fact, all faceted β-$SnWO_4$ microcrystals expose either {111} or {100} crystal planes or both together.[30] Therefore, cubes only exhibit {100} facets, whereas the tetrahedra only exhibit {111} facets (Table 2). Truncated tetrahedra and truncated octahedra expose both {111} and {100} crystal planes. The relative contribution of each type of crystal plane was estimated by statistical evaluation of microcrystals on SEM images. In the case of long-spiked spikecubes, the identification of the surface crystallography is not easy. The {100} planes of the pristine cubes are mainly covered by the spikes. The spikes—representing distortedly grown edges of cubes with (111) orientation—may contain {111} surfaces, but they will surely exhibit significant stress and strain due to their curvature. Due to these reactive surface sites and due to the high specific surface area (in comparison to all other microcrystals), long-spiked spikecubes show the second highest photocatalytic activity. Taken together, the photocatalytic activity of the β-$SnWO_4$ microcrystals, however, show a significantly higher activity of {111} over the {100} crystal surfaces (Table 2). Consequently, the β-$SnWO_4$ tetrahedra exhibit the highest activity for photocatalytic RhB decomposition of the presented microcrystals at all. Such a higher catalytic activity of {111} over {100} surfaces was often observed for oxides (e.g., Cu_2O, γ-Al_2O_3, Co_3O_4) and is related to the higher surface energy.[31−33]

CONCLUSIONS

Faceted β-$SnWO_4$ microcrystals are prepared for the first time with different morphologies such as tetrahedra, truncated tetrahedra, truncated octahedra, and short-spiked and long-spiked spikecubes. All of these morphologies are realized at very comparable experimental conditions via microwave-assisted synthesis of high-boiling alcohols (the so-called polyol method). Fundamental prerequisites for controlled growth are

Table 2. Comparison of the Relevant Material Properties and the Photocatalytic Activity of the As-Prepared Faceted β-$SnWO_4$ Microcrystals

morphology	average size (μm)	specific surface area (m^2/g)	ζ-potential (mV)	exposed crystal planes (according to SEM)	photocatalytic activity
truncated octahedra	4−6	1	−28	71% of {111} 29% of {100}	low
cubes	6−9	1	−43	{100} only	low
spikecubes (short-spiked)	7−10	1	−29	{100} plus spikes	low
truncated tetrahedra	10−16	1	−43	59% of {111} 41% of {100}	medium
spikecubes (long-spiked)	4−6	3	−37	{100} plus spikes	medium
tetrahedra	7−10	2	−24	{111} only	high

DOI: 10.1021/acsomega.9b01593
ACS Omega 2019, 4, 13400−13407

the use of $Na_2WO_4{\cdot}2H_2O$ as a starting material containing the same tetrahedral (WO_4) building unit as β-$SnWO_4$. The presence of water as mineralizer is essential as well, even at high temperatures (>150 °C). The conflicting issues of low temperature favoring controlled crystal growth and high temperature to guarantee the crystallinity of β-$SnWO_4$ were tackled by using a $Sn(OH)_2$ suspension as the starting material and the use of microwave-assisted heating. The slow dissolution of $Sn(OH)_2$ limits the available amount of Sn^{2+} during nucleation and serves as a reservoir for continuous release of Sn^{2+} during crystal growth. Fast microwave-assisted heating from the nucleation temperature (80 °C) to the growth temperature (170−220 °C) guarantees optimal crystallization and excludes the formation of additional amorphous nuclei that were obtained in the case of slow heating.

Based on the aforementioned optimal conditions of nucleation and growth, decisive parameters for well-controlled growth of faceted β-$SnWO_4$ microcrystals relate to the temperature of particle nucleation, the temperature, and time of particle growth, as well as the concentration of the starting materials. All obtained faceted microcrystals—tetrahedra, truncated tetrahedra, truncated octahedra, cubes, and short-spiked and long-spiked spikecubes—are exemplarily examined with regard to the photocatalytic degradation of rhodamine B. Due to the fact that several features of the microcrystals are very comparable (e.g., crystallinity, optical absorption and band gap, size, specific surface area, ζ-potential, and surface charging), the resulting photocatalytic performance can be directly correlated with the available crystal planes. Accordingly, {111} crystal planes clearly outperform {100} crystal planes, resulting in β-$SnWO_4$ tetrahedra as the most active microcrystals. As an outlook, these results, on the one hand, can trigger controlled growth and facet engineering of other metal oxides and, on the other hand, can support gaining deeper insights into photocatalytic and catalytic processes in general.

EXPERIMENTAL SECTION

Materials. Tin chloride ($SnCl_2{\cdot}2H_2O$, 98%, Sigma-Aldrich), sodium tungstate ($Na_2WO_4{\cdot}2H_2O$, 99%, Sigma-Aldrich), and diethylene glycol (DEG, $C_4H_{10}O_3$, 99%, Alfa Aesar) were used as purchased. The zwitterionic dye rhodamine B (RhB, $C_{28}H_{31}ClN_2O_3$, 99%, Acros Organics) was used as a model dye in photocatalytic dye degradation studies without further purification.

Synthesis of β-$SnWO_4$ Microcrystals. $Na_2WO_4{\cdot}2H_2O$ (0.75, 2.6, 3.6 mmol) was added to 150 mL of DEG at the nucleation temperature of 80 or 200 °C (T_N, Table 1) and stirred for 1 h for complete dissolution. The reaction was performed under argon flow to prevent any oxidation of DEG. An equimolar amount of $SnCl_2{\cdot}2H_2O$ (0.75, 2.6, 3.6 mmol) was added in 6 mL of deionized water, resulting in the formation of a turbid, colorless suspension of $Sn(OH)_2$. This suspension was injected into the solution of $Na_2WO_4{\cdot}2H_2O$ in DEG at the nucleation temperature of 80 or 200 °C. Thereafter, a yellow suspension was immediately formed and indicates the nucleation of β-$SnWO_4$. The preheated suspension was then placed in a microwave oven (operating at 1200 W) and heated fast (1 min) or slow (20 min) ($T_N \rightarrow T_G$, Table 1) to the growth temperature of 170−200 °C (T_G, Table 1). This growth temperature was kept for 30−60 min to support crystal growth. The growth of faceted β-$SnWO_4$ microcrystals is indicated by the brightening of the suspension originating from increased daylight reflection by the as-formed crystal-surface facets. Finally, the resulting suspension of faceted β-$SnWO_4$ microcrystals was washed three times with deionized water by sequential centrifugation and redispersion.

Characterization. *Microwave Oven.* Suspensions were heated in round-bottomed flasks with a magnetic stirrer under argon in a microwave oven (MLS rotaprep, operating at 1200 W) with a glass fiber (<200 °C) as well as a pyrometer (>200 °C) for temperature control.

Field emission scanning electron microscopy (FESEM, Zeiss Supra 40VP equipped with energy-dispersive X-ray spectrometer) was used to determine the morphology of the as-prepared faceted β-$SnWO_4$ microcrystals. The microcrystals were suspended in ethanol and dropped and dried on sliced pieces of a silicium wafer (5 × 5 mm^2).

Crystallinity and chemical composition of the faceted β-$SnWO_4$ microcrystals were examined by X-ray powder diffraction (XRD, Stoe STADI-MP diffractometer, equipped with Ge-monochromator and Cu $K\alpha_1$ radiation, 40 kV, 40 mA). About 10 mg of the microcrystals were deposited onto acetate foil and fixed with scotch tape.

UV−vis spectra of β-$SnWO_4$ microcrystals were recorded on a UV 2700 spectrometer (Shimadzu). For this, 4−8 mg of the microcrystals were mixed with 100−120 mg of dried $BaSO_4$ (spectroscopic grade) and measured against dried $BaSO_4$ as a reference. The determination of the band gap was done by the Kubelka−Munk formalism.

Photoluminescence spectroscopy was conducted with a Horiba Jobin Yvon Spex Fluorolog 3 (Horiba Jobin Yvon, France) equipped with a 450 W Xe-lamp and double grating excitation and emission monochromator. To detect certain emission, extremely broad slit widths of 5 nm for the excitation and emission monochromator were necessary.

Fourier-transform infrared (FT-IR) spectroscopy was performed with a Bruker Vertex 70 FT-IR spectrometer. For this, the microcrystals were grounded with dried KBr (1−2 mg with 400 mg KBr) and pressed for 15 min under 50 kN.

Volumetric nitrogen sorption measurements (BEL BEL-SORP-max) were carried out at 77 K with nitrogen as an analyte. According to the Brunauer−Emmett−Teller formalism the specific surface area was deduced. Prior to the analysis, the microcrystalline samples were dried at 120 °C in a vacuum.

To determine the ζ-potential of microcrystal β-$SnWO_4$ suspensions, Zetasizer Nano ZS from Malvern Instruments was used. About 1 mg of the microcrystals was suspended in water and ultrasonicated for 5 min prior to the analysis.

Photocatalytic Measurements. The photocatalytic dye degradation was carried out using a Shimadzu Excalibur measuring head linked with the aforementioned UV−vis spectrometer. For measurement, the quartz flask contained an aqueous suspension of the respective faceted β-$SnWO_4$ microcrystals (20 mg in 110 mL; 0.18 g/L) and the organic dye (0.20 mg/L). This suspension was continuously mixed with a magnetic stirrer. For photocatalytic degradation, a LOT Class ABA solar simulator (type LS0805) was applied that emits a spectrum of AM 1.5G solar light (100 mW/cm^2). Prior to illumination, the suspensions were magnetically stirred in the dark for 1 h to ensure homogenous distribution of the photocatalyst and the dye. All experiments were carried out at room temperature and in air. The course of the dye degradation was continuously monitored by comparing the intensity of the strongest absorption peak of the dye (λ_{RhB} =

DOI: 10.1021/acsomega.9b01593
ACS Omega 2019, 4, 13400−13407

554 nm) with the initial absorption at the beginning of the experiment. The obtained transmission−time plots were fitted by linear or allometric fits.

■ ASSOCIATED CONTENT

Supporting Information

The Supporting Information is available free of charge on the ACS Publications website at DOI: 10.1021/acsomega.9b01593.

Additional information on analytical characterization: optical properties of facetted β-$SnWO_4$ microcrystals, characterization of $Sn(OH)_2$, and optical properties of rhodamine B; Figures S1−S4 (PDF)

■ AUTHOR INFORMATION

Corresponding Author

*E-mail: claus.feldmann@kit.edu.

ORCID

Claus Feldmann: 0000-0003-2426-9461

Notes

The authors declare no competing financial interest.

■ ACKNOWLEDGMENTS

L.W. and C.F. are grateful to Deutsche Forschungsgemeinschaft (DFG) for funding of TEM equipment (INST 121384/33-1 FUGG). Moreover, we thank the Helmholtz-Program Science and Technology of Nanosystems (STN), subtopic Nanocatalysis, for support and collaboration. L.W., finally, acknowledges Studienstiftung des deutschen Volkes for scholarship.

■ REFERENCES

(1) Huang, M. H. Facet-Dependent Optical Properties of Semiconductor Nanocrystals. *Small* **2019**, *15*, No. 1804726.

(2) Liu, G.; Yu, J. C.; Lu, G. Q.; Cheng, H.-M. Crystal Facet Engineering of Semiconductor Photocatalysts: Motivations, Advances and Unique Properties. *Chem. Commun.* **2011**, *47*, 6763−6783.

(3) Xia, Y.; Gilroy, K. D.; Peng, H.-C.; Xia, X. Seed-Mediated Growth of Colloidal Metal Nanocrystals. *Angew. Chem., Int. Ed.* **2017**, *56*, 60−95.

(4) Wang, Y.; He, J.; Liu, C.; Chong, W. H.; Chen, H. Thermodynamics Versus Kinetics in Nanosynthesis. *Angew. Chem., Int. Ed.* **2015**, *54*, 2022−2051.

(5) Kadam, A. N.; Kim, T. G.; Shin, D. S.; Garadkar, K. M.; Park, J. Morphological Evolution of Cu Doped ZnO for Enhancement of Photocatalytic Activity. *J. Alloys Compd.* **2017**, *710*, 102−113.

(6) Harn, Y.-W.; Yang, T.-H.; Tang, T.-Y.; Chen, M.-C.; Wu, J.-M. Crystals with Controlled Morphology. *ChemCatChem* **2015**, *7*, 80−86.

(7) Mann, A. K. P.; Fu, J.; DeSantis, C. J.; Skrabalak, S. E. Spatial and Temporal Confinement of Salt Fluxes for the Shape-Controlled Synthesis of Fe_2O_3 Nanocrystals. *Chem. Mater.* **2013**, *25*, 1549−1555.

(8) Xiao, X.; Liu, X.; Zhao, H.; Chen, D.; Liu, F.; Xiang, J.; Hu, Z.; Li, Y. Facile Shape Control of Co_3O_4 and the Effect of the Crystal Plane on Electrochemical Performance. *Adv. Mater.* **2012**, *24*, 5762−5766.

(9) Yang, P. Surface Chemistry. Crystal Cuts on the Nanoscale. *Nature* **2012**, *482*, 41−42.

(10) Foo, G. S.; Hood, Z. D.; Wu, Z. Shape Effect Undermined by Surface Reconstruction: Ethanol Dehydrogenation over Shape-Controlled $SrTiO_3$ Nanocrystals. *ACS Catal.* **2018**, *8*, 555−565.

(11) Huang, M. H.; Rej, S.; Hsu, S.-C. Facet-dependent Properties of Polyhedral Nanocrystals. *Chem. Commun.* **2014**, *50*, 1634−1644.

(12) Tsai, Y.-H.; Chanda, K.; Chu, Y.-T.; Chiu, C.-Y.; Huang, M. H. Direct Formation of Small Cu_2O Nanocubes, Octahedra, and Octapods for Efficient Synthesis of Triazoles. *Nanoscale* **2014**, *6*, 8704−8709.

(13) Cordeiro, M. A. L.; Weng, W.; Stroppa, D. G.; Kiely, C. J.; Leite, E. R. High Resolution Electron Microscopy Study of Nanocubes and Polyhedral Nanocrystals of Cerium(IV) Oxide. *Chem. Mater.* **2013**, *25*, 2028−2034.

(14) D'Arienzo, M.; Carbajo, J.; Bahamonde, A.; Crippa, M.; Polizzi, S.; Scotti, R.; Wahba, L.; Morazzoni, F. Photogenerated Defects in Shape-Controlled TiO_2 Anatase Nanocrystals: A Probe To Evaluate the Role of Crystal Facets in Photocatalytic Processes. *J. Am. Chem. Soc.* **2011**, *133*, 17652−17661.

(15) Chen, J.; Burger, C.; Krishnan, C. V.; Chu, B. Morphogenesis of Highly Ordered Mixed-Valent Mesoporous Molybdenum Oxides. *J. Am. Chem. Soc.* **2005**, *127*, 14140−14141.

(16) Liu, Y.; Yang, D.; Yu, R.; Qu, J.; Shi, Y.; Li, H.; Yu, Z.-Z. Tetrahedral Silver Phosphate/Graphene Oxide Hybrids as Highly Efficient Visible Light Photocatalysts with Excellent Cyclic Stability. *J. Phys. Chem. C* **2017**, *121*, 25172−25179.

(17) Yang, Y. A.; Wu, H.; Williams, K. R.; Cao, Y. C. Synthesis of CdSe and CdTe Nanocrystals Without Precursor Injection. *Angew. Chem., Int. Ed.* **2005**, *44*, 6712−6715.

(18) Ungelenk, J.; Feldmann, C. Synthesis of Faceted β-$SnWO_4$ Microcrystals and Enhanced Visible-light Photocatalytic Properties. *Chem. Commun.* **2012**, *48*, 7838−7840.

(19) Noureldine, D.; Takanabe, K. State-of-the-art Sn^{2+}-based Ternary Oxides as Photocatalysts for Water Splitting: Electronic Structures and Optoelectronic Properties. *Catal. Sci. Technol.* **2016**, *6*, 7656−7670.

(20) Iwase, A.; Yoshino, S.; Takayama, T.; Ng, Y. H.; Amal, R.; Kudo, A. Water Splitting and CO_2 Reduction under Visible Light Irradiation Using Z-Scheme Systems Consisting of Metal Sulfides, CoO_x-Loaded $BiVO_4$, and a Reduced Graphene Oxide Electron Mediator. *J. Am. Chem. Soc.* **2016**, *138*, 10260−10264.

(21) Kudo, A.; Miseki, Y. Heterogeneous Photocatalyst Materials for Water Splitting. *Chem. Soc. Rev.* **2009**, *38*, 253−278.

(22) Nosaka, Y.; Nosaka, A. Y. Generation and Detection of Reactive Oxygen Species in Photocatalysis. *Chem. Rev.* **2017**, *117*, 11302−11336.

(23) Jeitschko, W.; Sleight, A. W. The Crystal Structure of $HgMoO_4$ and two Forms of $SnWO_4$. *Z. Naturforsch., B: J. Chem. Sci.* **1971**, 203.

(24) Ungelenk, J.; Feldmann, C. Nanoscaled Tin Tungstate − A Highly Efficient Photocatalyst for Daylight-driven Degradation of Organic Dyes and Its Quick and Easy Synthesis. *Appl. Catal., B* **2011**, *102*, 515−520.

(25) Dong, H.; Chen, Y.-C.; Feldmann, C. Polyol Synthesis of Nanoparticles: Status and Options regarding Metals, Oxides, Chalcogenides, and Non-Metal Elements. *Green Chem.* **2015**, *17*, 4107−4132.

(26) Seidl, C.; Ungelenk, C.; Zittel, E.; Bergfeldt, T.; Sleeman, J. P.; Schepers, U.; Feldmann, C. Tin Tungstate Nanoparticles: A Photosensitizer for Photodynamic Tumor Therapy. *ACS Nano* **2016**, *10*, 3149−3157.

(27) Chen, Y.-C.; Lin, Y.-G.; Hsu, L.-C.; Tarasov, A.; Chen, P.-T.; Hayashi, M.; Ungelenk, J.; Hsu, Y.-K.; Feldmann, C. β-$SnWO_4$ Photocatalyst with Controlled Morphological Transition of Cubes to Spikecubes. *ACS Catal.* **2016**, *6*, 2357−2367.

(28) Wojcik, J.; Calvayrac, F.; Goutenoire, F.; Mhadhbi, N.; Corbel, G.; Lacorre, P.; Bulou, A. Lattice Dynamics of β-$SnWO_4$. *J. Phys. Chem. C* **2013**, *117*, 5301−5313.

(29) LaMer, V. K.; Dinegar, R. H. Theory, Production and Mechanism of Formation of Monodispersed Hydrosols. *J. Am. Chem. Soc.* **1950**, *72*, 4847−4854.

(30) Hermann, K. *Crystallography and Surface Structure: An Introduction for Surface Scientists and Nanoscientists*; Wiley-VCH: Weinheim, 2016.

DOI: 10.1021/acsomega.9b01593
ACS Omega 2019, 4, 13400−13407

(31) Song, Y.-Y.; Wang, G.-C. Theoretical Study of Propylene Epoxidation over $Cu_2O(111)$ Surface: Activity of O^{2-}, O^{-}, and O^{2-} Species. *J. Phys. Chem. C* **2018**, *122*, 21500−21513.
(32) Wang, Y.; Yang, J.; Gu, R.; Peng, L.; Guo, X.; Xue, N.; Zhu, Y.; Ding, W. Crystal-Facet Effect of γ-Al_2O_3 on Supporting CrO_x for Catalytic Semihydrogenation of Acetylene. *ACS Catal.* **2018**, *8*, 6419−6425.
(33) Liu, L.; Jiang, Z.; Fang, L.; Xu, H.; Zhang, H.; Gu, X.; Wang, Y. Probing the Crystal Plane Effect of Co_3O_4 for Enhanced Electrocatalytic Performance toward Efficient Overall Water Splitting. *ACS Appl. Mater. Interfaces* **2017**, *9*, 27736−27744.

DOI: 10.1021/acsomega.9b01593
ACS Omega 2019, 4, 13400−13407